Peer-reviewed version available at *Crystals* **2018**, *8*, 324; doi:10.3390/cryst8080324

Stress relaxation properties and microscopic deformation structure in bending of the C7025 and C7035 alloy

Xiang P. Xiao [a*], Hai Xu [a], Jian Huang [b], Jun F. Wang [b], Jian B. Zhang [a**]

[a] Jiangxi University of Science and Technology, Institute of Engineering Research, Hongqi Ave. No.86, 341000 Ganzhou, China;

[b] Jiangxi University of Science and Technology, School of Materials Science and Engineering, Hongqi Ave. No.86, 341000 Ganzhou, China.

*** Correspondence authors:**

Professor Xiang P. Xiao

E-mail: xiao_xiangpeng@126.com Tel.:+86(797)8312705

Professor Jian B. Zhang

E-mail: zhang4318@163.com Tel.:+86(797)8312705

Abstract

Stress relaxation tests in cantilever bending were performed on the C7025 and C7035 alloys at 298K and 393K，respectively. The effect of stress-relief treatments on stress relaxation properties was investigated. The structural changes associated with the stress relaxation process were examined using transmission electron microscope. The stress relaxation curve fits well to empirical formula $\sigma^*=[K'\ln(t+\alpha_0)+C]^{-n}$ for stress relaxation. The curves can be split into two stages. The stress relax quickly in the first stage, slows down in the second stage, and tends to be a certain limit value after a long time. The curve and microstructure reveals that the C7035 alloy has a lower rate of stress relaxation and a higher anti-stress relaxation capacity than the C7025. The first reason is that the movement of vacancies required by spinodal decomposition is inhibited, and the quantity of cobalt -containing vacancies decreases dramatically in the C7035 alloy. The other reason is that the precipitated phases became uniformly diffused in the C7035 alloy. The precipitate phase uniformly distributes in the grain boundaries and the matrix, during the relaxed condition, and thus the dislocations moving is blocked by the precipitates.

Key words: C7025 alloy; C7035 alloy; stress relaxation; dynamic equation; microstructure

1. Introduction

C7025 alloys are widely used in the fabrication of conductor components and lead frame materials due to their excellent strength and conductivity [1-3]. However, C7035 alloys have higher strength, electrical conductivity and more appropriate stress relaxation properties [4-5]. The quality of materials used to construct lead frames and the conductors in components can be determined by their elastic limit and relaxation stability. Stress relaxation is a distinct type of deformation, in which elastic strain changes to plastic strain under the action of thermal activation and stress [6-7]. The stress relaxation and creep exhibit some similarity in observed phenomena and it was concluded that the nature of stress relaxation corresponds to creep behavior, so stress relaxation is generally explained using creep theory [8]. The stress relaxation properties of the copper alloy at room temperature after a cold rolling test, concluded that recovery and relaxation processes were similar, as dislocation motion, rearrangements and the number of movable dislocations had decreased [9]. Due to the effects of elastic stress, uphill diffusion of beryllium atoms occurred leading to Guinier-Preston (GP) zone formation, thus improving the stress relaxation properties of the alloy at room temperature and leading to stable performance when studied the stress relaxation behavior of beryllium copper [10]. It is important to characterize the stress relaxation behavior of elastic copper alloy not only in terms of the remaining stress after exposure to elevated temperatures, but also in terms of microstructural changes. The purpose of this paper is to present the results of low temperature stress relaxation tests performed with C7025 and C7035 alloys and attempt to ascertain the mechanism of microscopic deformation.

2. Experimental

The materials selected for this study were C7025 and C7035 alloys in the form of plates with a thickness of 0.3 mm in a cold-rolled condition. The chemical composition of the alloys is shown in Table 1. Stress relaxation testing was carried out according to ASTM E328-78 standard method for plate products. The specimens for stress relaxation (Figure 1) were cut parallel to the rolling direction of the plate, using spark machinery from stock

samples. Stress relaxation was performed at room temperature (298K) and at 393K in a furnace, respectively.

Tensile testing was carried out on a WE-30 hydraulic universal material testing machine. Transmission electron microscopy samples were prepared using a conventional electro-polishing method with an electrolyte of 25 vol.% HNO_3 and 75 vol% CH_3OH at -30℃. A JEM 2100 LaB6 transmission electron microscopy operating at 200 kV was employed to image the microstructure of the samples.

3. Calculation

During stress relaxation, the total strain (ε_t) remains constant. ε_t can be expressed as follows:

$$\varepsilon_t=\sigma_0/E_c=\text{const} \quad (1)$$

where σ_0 is the initial stress and E_c is the modulus of the specimen.

Total strain (ε_t) can be expressed as the sum of the elastic strain (ε_c) and inelastic strain (ε_p) [11]:

$$\varepsilon_t=\varepsilon_c+\varepsilon_p \quad (2)$$

So, inelastic strain (ε_p) can be expressed as:

$$\varepsilon_p=\varepsilon_t-\varepsilon_c=(\sigma-\sigma_0)/E \quad (3)$$

After differentiation, Equation (3) becomes:

$$\dot{\varepsilon} = -\frac{d\sigma}{E_c dt} \quad (4)$$

In terms of the dislocation theory outlined by Orowan, the relationship between the rate of strain and the dislocation density can be expressed as:

$$\dot{\varepsilon}_p = \Phi\rho_m b\nu \quad (5)$$

where Φ is the angle of the direction of dislocation, ρ_m is the mobile dislocation density, b is the Burgers vector and ν is the average dislocation.

According to the semi-empirical observations of Johnston and Gilman, the average dislocation (ν) can be expressed as:

$$\nu=B(\sigma^*)^m \quad (6)$$

Preprints (www.preprints.org) | NOT PEER-REVIEWED | Posted: 5 July 2018 doi:10.20944/preprints201807.0080.v1

Peer-reviewed version available at Crystals 2018, 8, 324; doi:10.3390/cryst8080324

where B and m are material constants for the test temperature respectively and σ* is the effective stress, which is defined as the difference between applied stress σ and long range internal stress σ_i:

$$\sigma^*=\sigma-\sigma_i \tag{7}$$

When atomic organization remain unchanged during relaxation, in order to facilitate the calculation, σ_i is treated as constant.

Taking the derivative of both sides with respect to t in equation (7) results in:

$$\dot{\sigma}^* = \dot{\sigma} \tag{8}$$

Combining equations (4), (5), (6) and (8), the following equation can be obtained:

$$\dot{\sigma}^* = -\Phi E_c \rho_m bB\left(\sigma^*\right)^m \tag{9}$$

The following discussion will be divided into two parts.

(i) It is assumed that the mobile dislocation density (ρ_m) will be unchanged during relaxation. Therefore ρ_m is treated as constant, so $d\rho_m/dt=0$ and equation (9) can be expressed as [12]:

$$\sigma^*=(Kt+\alpha)^{-n} \tag{10}$$

where:

$$K=(m-1)\ \Phi E_c \rho_m bB \tag{10a}$$

$$n=1/(m-1) \tag{10b}$$

$$\alpha=\sigma_0{}^{*(1-m)} \tag{10c}$$

(ii) It is assumed that the mobile dislocation density (ρ_m) decreases with time:

$$\rho_m(t) = A/(t+\alpha_0) \tag{11}$$

where, $\rho_m(t)$ is the mobile dislocation density at a certain time during relaxation. A and α_0 are material constants at the test temperature respectively.

On integrating, equation (9) can be expressed as:

$$\sigma^*=[K'\ln(t+\alpha_0)+C]^{-n} \quad (12)$$

where:

$$K'=(m-1)\ \Phi E_c bBA \quad (12a)$$

$$C=\sigma_0{}^{*(1-m)} -(m-1)\ \Phi E_c bBA\ \ln\alpha_0 \quad (12b)$$

4. Results

4.1 Dynamic equation of stress relaxation

The mechanical properties of C7025 and C7035 alloys at room-temperature in aging-cold-rolled conditions is listed in Table1. Fifty percent of the elastic limit stress was used to set the initial stress for stress relaxation tests. The specimens were flexed to the desired initial stress level at 298K and 393K. The spring back deflection was proportional to the constraining force. Hence, by measuring permanent set as a function of time, the relationship between the remaining stress and time can be calculated.

Stress relaxation curves for C7025 and C7035 alloys at 298 K and 393K are shown in Figure 2. The curves are split into two stages. Stress relaxation occurred quickly in the first stage and slowly in the second stage, tending to a certain limit value after a long time.

Numerical results after applying equations (10) and (12) for the stress relaxation data of C7025 and C7035 at different stress-relief treatments for relaxation at 298K and 393K are shown in Table 3. It can be seen from the results that the curve fits well with the empirical formula for stress relaxation.

4.2 Transmission electron microscopy analysis of relaxed specimens

4.2.1 Before stress relaxation

Discontinuous precipitation occurred along the grain boundaries, shown in Figure 3 (a) and (b). The extent of discontinuous precipitation in the C7025 alloy was greater than in the C7035 alloy. As temperature and aging time increasing, the cellular structures formed by discontinuous precipitation in the C7025 alloy underwent nucleation

along the grain boundaries, including in-growth into the grains. Attachment of cellular structures onto the sub-boundaries caused a reduction in the resistance to mobile dislocation and an increase in the propensity for glide and climb. This finally results in a reduction in anti-stress-relaxation capacity. The diffraction patterns for Figure 3 (a) and (b) are showed as Figure 3 (c) and (d), respectively. Figure 3 (e) and (f) demonstrate that the second-phase particles were distributed intragranularly and along the grain boundaries, hindering the movement of dislocations. Relationship of the crystal orientations between matrix and precipitates follows $[011]_{matrix}$ //$[111]_{precipitate}$, $(-11-1)_{matrix}$ //$(10-1)_{precipitate}$; $[-112]_{matrix}$ //$[32-4]_{precipitate}$, $(110)_{matrix}$ //$(2-11)_{precipitate}$.

4.2.2 After stress relaxation

Compared with transmission electron microscopy images before relaxation, it can be seen from Figure 4, dislocation density decreased significantly after stress relaxation. This indicates that after long-term stress relaxation, dislocation glide and climb occurred, with parallel alignment of dislocations of the same sign along the grain boundaries and sub-boundaries and offset of dislocations with opposite signs. In the C7035 alloy, partial substitution of nickel by cobalt promoted the precipitation of the second phase and twinning in the matrix. These phenomena have the effect of preventing dislocation. A comparison of transmission electron microscopy images of C7035 alloy with that of the C7025 alloy after stress relaxation for 100h reveals the presence of twinning in the C7035 alloy (indicated by A in Figure 4 (a)). For a dislocation to glide away from the twinning, greater energy is required. This is the reason that twinning prevents dislocation, reducing the rate of stress relaxation in alloys and increasing the anti-stress relaxation capacity of the material. Significant discontinuous precipitation occurred in C7025 alloy, leading to the formation of cellular structures and a reduction in resistance to mobile dislocation along the sub-boundaries during stress relaxation. This further promoted glide and climb, increasing the rate of stress relaxation, and reducing anti-stress relaxation capacity. Besides discontinuous precipitation, dynamic recovery and recrystallization (indicated by B in Figure 4 (b)) were observed in C7025 alloy during long-term stress relaxation. This process caused further reduction in stress and hence a decline in the anti-stress relaxation

capacity. As shown in Figure 4, partial substitution of nickel by cobalt element in C7035 alloy promoted the formation of a precipitated phase and twinning, hindering discontinuous precipitation and mobile dislocation during stress relaxation. This further improved the anti-stress relaxation capacity of the material.

As relaxation temperature increased, the resistance to mobile dislocation decreased. In Figure 5, the interaction between dislocation and second-phase particles can be seen in the bending of dislocations pinned by adjacent second-phase particles. Streak structures appeared in the C7035 alloy (indicated by A in Figure 5 (a)). These hindered the movement of dislocations, which were confined to the area between the streaks. Recrystallized structures occurred in the grains after stress relaxation of the C7025 alloy at high temperature for a long period of time (indicated by B in Figure 5 (a)), which further reduced stress and caused a decline in anti-stress relaxation capacity of the material.

5. Discussion

During the first stage of stress relaxation, the rate of relaxation is faster because of the accelerated rate of dynamic recovery and recrystallization. Interactions between vacancies, dislocations of the same and opposite sign accelerate realignment and movement of dislocations. Furthermore, at this stage of stress relaxation, a large number of mobile dislocations accumulate inside the grains, which reduces the resistance to mobile dislocation. For the above reasons, the anti-stress relaxation capacity at this stage is greatly reduced. The rate of stress relaxation is lower during the second stage of stress relaxation, when interactions between dislocations, second-phase particles and impurities cause multiplication of dislocations. As a result, the movement of dislocations is hindered. Transmission electron microscopy images show that the sub-grains are not formed uniformly along the grain boundaries and sub-boundaries, but concentrated locally. This causes heterogeneous deformation after stress relaxation (Figure 4). Because of hindered movement of dislocations in the regions of micro-plastic deformation, the pile-up of dislocations is observed, leading to stress concentration. Therefore, during the second stage of stress relaxation, the relaxation is caused by dislocation glide under high stress, which

occurs at a lower rate. That explains the low rate of stress relaxation during the second stage [13-15].

Compared with the C7025 alloy, the C7035 alloy has a lower rate of stress relaxation and a higher anti-stress relaxation capacity. The presence of doped cobalt reduced the tendency towards spinodal decomposition because the solid solubility of cobalt in copper is lower and cobalt is likely to bind to available vacancies. As a result, the movement of vacancies required by spinodal decomposition was inhibited [4], and the quantity of cobalt-containing vacancies decreased dramatically in the C7035 alloy. This further inhibited the glide of mobile dislocations and improved the anti-stress relaxation capacity. Furthermore, doped cobalt promoted precipitation from the matrix, the precipitated phases becoming uniformly diffused in the alloy matrix. During the process of stress relaxation, mobile dislocations were pinned by the second-phase particles in diffuse distribution. A stable Cottrell atmosphere was formed around the second-phase particles, so that dislocation clusters hindered the movement of the mobile dislocations, increasing anti-stress relaxation capacity while reducing the degree of stress relaxation. The precipitated phases were uniformly distributed along the grain boundaries and in the matrix. Mobile dislocations can move during stress relaxation until being pinned by the second-phase particles, which gives rise to the Cottrell atmosphere. As mobile dislocations deposit to form dislocation clusters, their movement is made difficult during the process of stress relaxation [16-18]. For these reasons, the degree of stress relaxation decreases, and so anti-stress relaxation capacity increases.

6. Conclusions

(1) The stress relaxation curves of the C7025 and C7035 alloys can be described in empirical formula of $\sigma^*=[K'\ln(t+\alpha_0)+C]^{-n}$ with great precision.

(2) The stress relaxation curves are split into two stages. Stress relaxed quickly in the first stage and slows down in the second stage and tends to a certain limit value after a long time. At the first stage of stress relaxation, a large quantity of mobile dislocations accumulate inside the grains, which reduces the resistance to mobile dislocation. Second-phase particles and impurities cause multiplication of dislocations in the second stage which

lead a lower rate of stress relaxation.

(3) The C7035 alloy has a lower rate of stress relaxation and a higher anti-stress relaxation capacity than the C7025 alloy. On one hand, this is because that the movement of vacancies required by spinodal decomposition is inhibited, and the quantity of cobalt -containing vacancies decrease dramatically in the C7035 alloy. On the other hand, the precipitated phases becoming uniformly diffuse in the C7035 alloy.

Acknowledgement

This work was supported by the National Natural Science Foundation of China (No. 51561008 and 51461017) and Key Program of Jiangxi Natural Science Foundation for Young Scholar(No. 20171ACB21044 and 20161BBE50030). Special thanks are given to professor Liu Ruiqing and Dr. Wang Hang for enlightening discussions.

References

[1] S. SUZUKI, N.SHIBUTANI, K. MIMURA, M. ISSHIKI, Y. WASEDA, Improvement in strength and electrical conductivity of Cu-Ni-Si alloys by aging and cold rolling, J. Alloys Comd., 417 (2006) 116-120.

[2] R. MONZEN, C. WATANABE, Microstructure and mechanical properties of Cu-Ni-Si alloys, Mater. Sci. Eng. A., 482 (2008) 117-123.

[3] K. Izawa , A. Ozawa, K. Kita, C. Watanabe, R. Monzen, Influence of Co on strength and microstructure of Cu-Ni-Co-Si alloy, J. Soc. Mater. Sci. Japan., 63 (2014) 401-408.

[4] X.P. Xiao, Z.Y. Yi, T.T. Chen, R.Q. Liu, H. Wang, Suppressing spinodal decomposition by adding Co into Cu-Ni-Si alloy, J. Alloys Comd., 660 (2016) 178-183.

[5] Q.S. Wang, G.L. Xie, X.J. Mi, B.Q. Xiong, X.P. Xiao, The precipitation and strengthening mechanism of Cu-Ni-Si-Co alloy, Chinese Mater. Conf., 749 (2012) 294-298.

[6] J.F. Chen, J.T. Jiang, L. Zhen, Stress relaxation behavior of an Al-Zn-Mg-Cu alloy in simulated age-forming process, J. Mater. Process. Technol., 214 (2014) 775-783.

[7] X.X. Xu, X.Y. San, Y.L. Gong, Studies on strength and ductility of Cu-Zn alloys by stress relaxation, Mater. Des., 47 (2013) 295-299.

[8] H. D. Chandler, A comparison between steady state creep and stress relaxation in copper, Mater. Sci. Eng. A., 527 (2010) 6219-6223.

[9] Parikin, Stress Relaxation Testing, ASTM, (1979) 48-53.

[10] Y.L. Li, Y.J. Han, S.C.Yu, Stress relaxation properties and microstructure of Cu-Be alloys, Trans. Nonferrous Met. Soc. China., 3 (1993) 62-65.

[11] L. Xiao, J.L. Bai, Stress relaxation properties and microscopic deformation structure of H68 and QSn6.5-0.1 copper alloys at 353 K, Mater. Sci. Eng. A., 244 (1998) 250-256.

[12] J.C.M. Li, Dislocation dynamics in deformation and recovery, Can. J. Phys., 45 (1967) 493-509.

[13] P. Virtanen, Stress relaxation behavior in bending of high strength copper alloys in the Cu-Ni-Sn system, Mater. Sci. Eng. A., 238 (1997) 407-420.

[14] F. Povolo, R.Tinivella, Stress relaxation in bending of type AISI 304 and A-286 steels at 773K, J. Mater. Sci., 19 (1984) 1851-1862.

[15] D.H. Lee, S.W. Nam, S.J. Choe, Effect of microstructure and relaxation behavior on the high temperature low cycle fatigue of near-α-Ti-1100, Mater. Sci. Eng. A., 291 (2000) 60-67.

[16] I.A. Povarov, Stress relaxation in structural titanium alloys, Met. Sci. Heat Treat., 22 (1982) 433-452.

[17] T. Mori, Diffusional relaxation around a second phase particle, Acta Metall., 28 (1980) 319-321.

[18] S.Onaka, Kinetics of Stress relaxation caused by the combination of interfacial sliding and diffusiong:Two-dimensional analysis, Acta Mater., 46 (1998) 3821-3830.

Preprints (www.preprints.org) | NOT PEER-REVIEWED | Posted: 5 July 2018 doi:10.20944/preprints201807.0080.v1

Peer-reviewed version available at Crystals 2018, 8, 324; doi:10.3390/cryst8080324

Table 1 Composition for the experimental alloy

Alloy	Nickel	Silicon	Cobalt	Copper
C7025	2.6	0.6	0	Balance
C7035	1.4	0.6	1.2	Balance

Table 2 Mechanical properties of C7025 and C7035 alloys in aging-cold-rolled conditions

Alloy	Tensile strength σ_b (MPa)	Yield strength σ_s (MPa)	Elongation δ (%)
C7025	756	535	5
C7035	838	584	5

Table 3 Test results after applying the empirical equation

Alloy	Temperature	Dynamic equation	Variance	Correlation coefficient
C7035	298K	$\sigma^*=449.96+75.75\times(t+1.61)^{-0.16}$	3.19	0.989
	393K	$\sigma^*=108.98+401.91\times(t+0.28)^{-0.02}$	8.71	0.978
C7025	298K	$\sigma^*=367.44+142.56\times(t+0.31)^{-0.06}$	5.31	0.988
	393K	$\sigma^*=63.18+433.9\times(t+0.03)^{-0.02}$	5.02	0.992
C7035	298K	$\sigma^*=[1.23\times10^{-6}+4.47\times10^{-8}\times(t+0.95)]^{-0.46}$	2.89	0.991
	393K	$\sigma^*=[8.27\times10^{-7}+2.82\times10^{-8}\times(t+0.36)]^{-0.45}$	8.28	0.979
C7025	298K	$\sigma^*=[1.31\times10^{-6}+4.42\times10^{-8}\times(t+0.28)]^{-0.46}$	5.30	0.988
	393K	$\sigma^*=[8.54\times10^{-7}+2.68\times10^{-8}\times(t+0.05)]^{-0.45}$	4.86	0.992

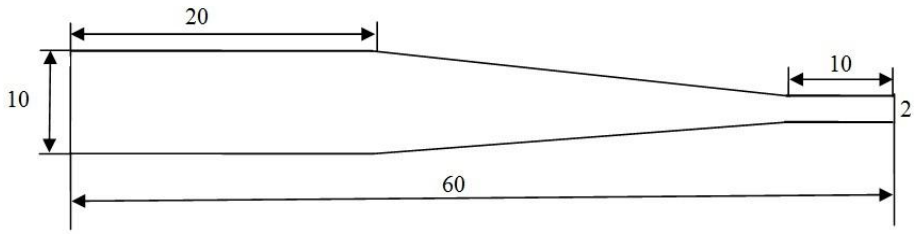

Figure 1: Shape and size of stress relaxation specimen (unit: mm)

Preprints (www.preprints.org) | NOT PEER-REVIEWED | Posted: 5 July 2018 doi:10.20944/preprints201807.0080.v1

Peer-reviewed version available at Crystals 2018, 8, 324; doi:10.3390/cryst8080324

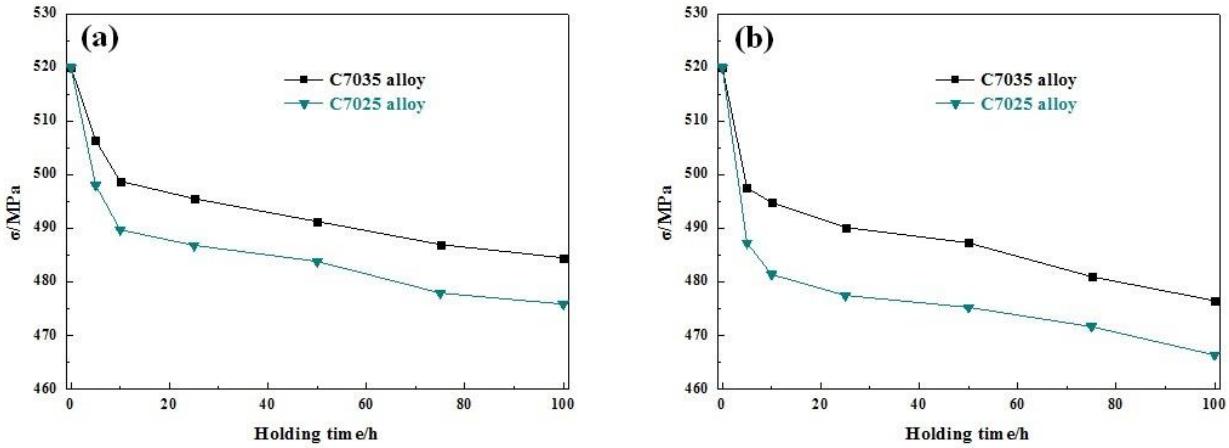

Figure 2: Stress relaxation curves for the C7025 and C7035 alloys at 298 K (a) and 393K (b)

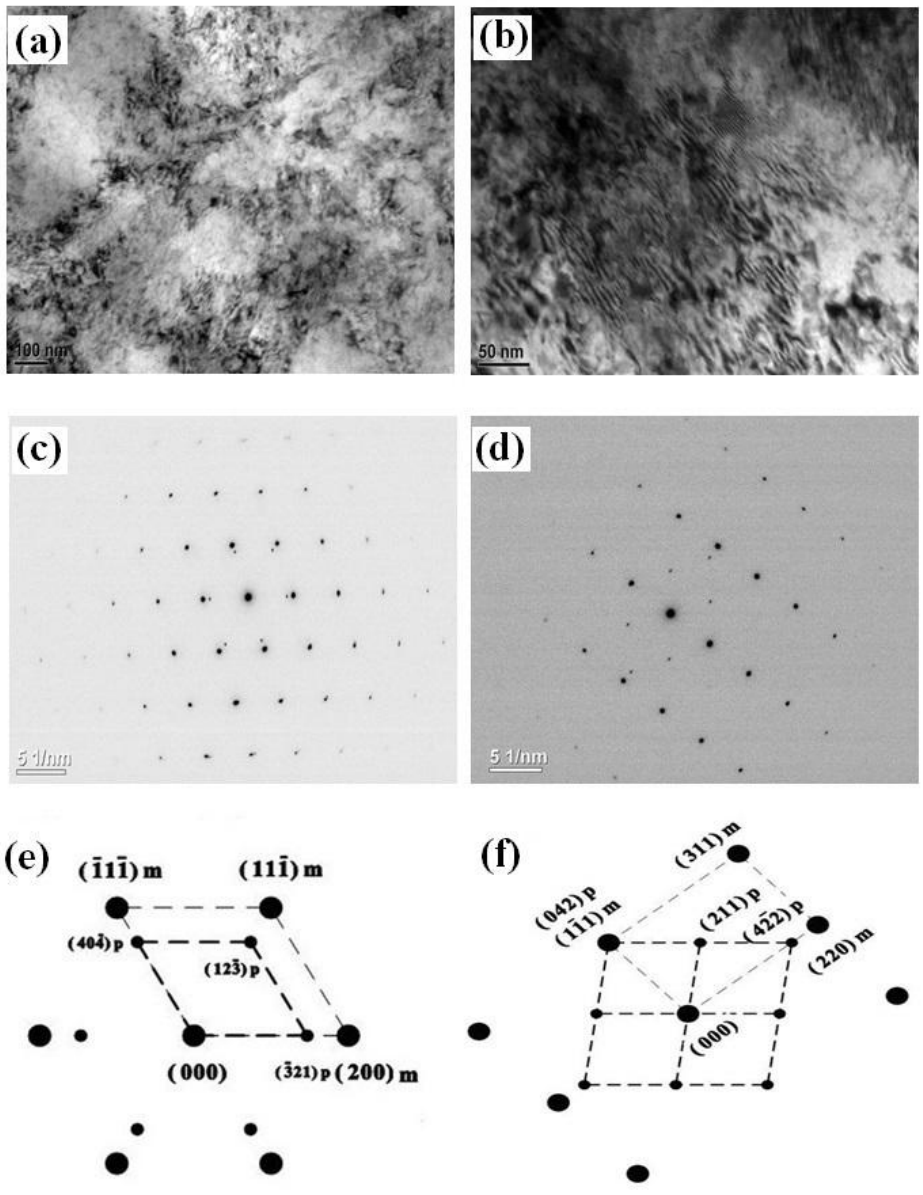

Figure 3: The organization of before stress relaxation (a) transmission electron microscopy image of the C7035

alloy; (b) transmission electron microscopy image of the C7025 alloy;(c) selected area diffraction patter of (a); (d) selected area diffraction patter of (b); (e) result of (c); (f) result of (d)

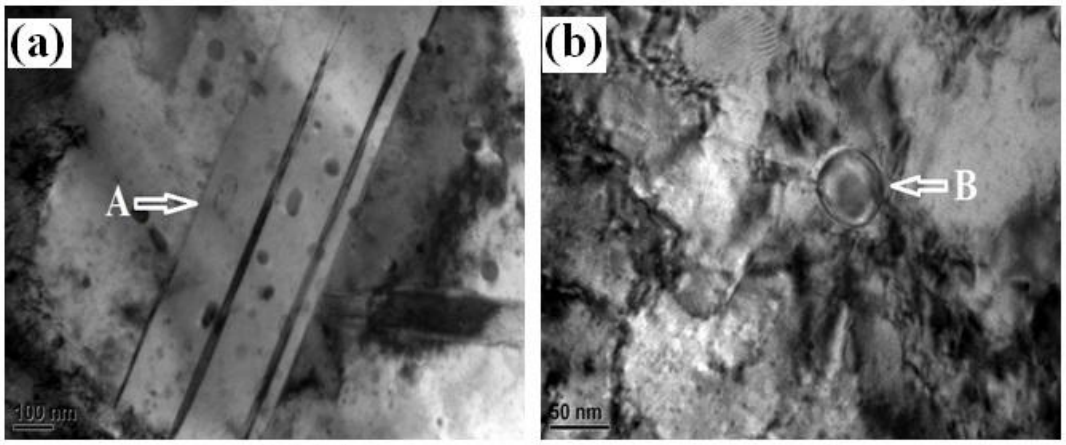

Figure 4: Transmission electron microscopy images of stress relaxation after 100h at 298K (a) the C7035 alloy; (b) the C7025 alloy

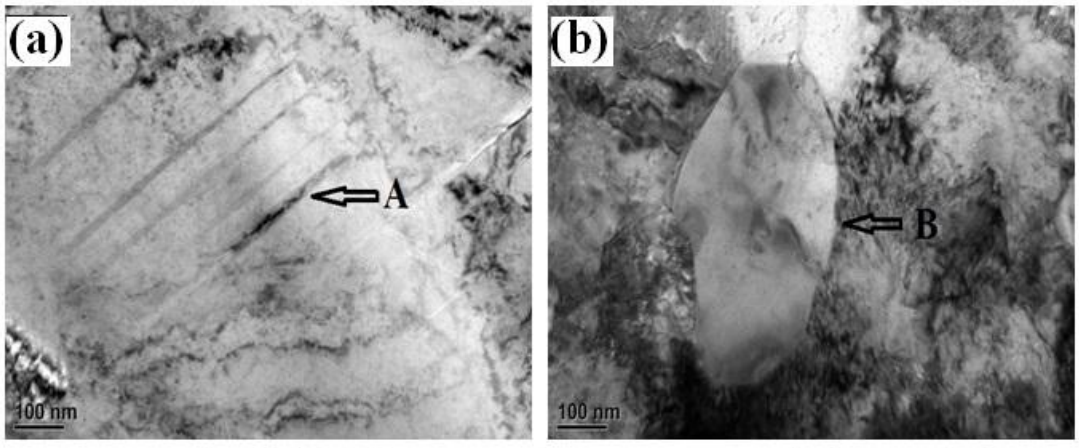

Figure 5: Transmission electron microscopy images of stress relaxation after 100h at 393K (a) the C7035 alloy; (b) the C7025 alloy